Inorganic Chemistry

Article

pubs.acs.org/IC

Co-ligand and Solvent Effects on the Spin-Crossover Behaviors of PtS-type Porous Coordination Polymers

Xiang-Yi Chen, Rong-Bin Huang, Lan-Sun Zheng, and Jun Tao*

State Key Laboratory of Physical Chemistry of Solid Surfaces and Department of Chemistry, College of Chemistry and Chemical Engineering, Xiamen University, Xiamen 361005, People's Republic of China

Supporting Information

ABSTRACT: In our previous work (Chen, X.-Y.; et al. *Chem. Commun.* **2013**, *49*, 10977−10979), we have reported the crystal structure and spin-crossover properties of a compound $[Fe(NCS)_2(tppm)]\cdot S$ [**1**·*S*, tppm = 4,4′,4″,4‴-tetrakis(4-pyridylethen-2-yl)tetraphenylmethane, $S = 5CH_3OH\cdot 2CH_2Cl_2$]. Here, its analogues $[Fe(X)_2(tppm)]\cdot S$ [X = $NCSe^-$, $NCBH_3^-$, and $N(CN)_2^-$ for compounds **2**·*S*, **3**·*S*, and **4**·*S*, respectively] have been synthesized and characterized by variable-temperature X-ray diffraction and magnetic measurements. The crystal structure analyses of **2**·*S* and **3**·*S* reveal that both compounds possess the same topologic framework (PtS-type) building from the tetrahedral ligand tppm and planar unit FeX_2; the framework is two-fold self-interpenetrated to achieve one-dimensional open channels occupied by solvent molecules. Powder X-ray diffraction study indicates the same crystal structure for **4**. The average values of Fe−N distances observed, respectively, at 100, 155, and 220 K for the Fe1/Fe2 centers are 1.969/2.011, 1.970/2.052, and 2.098/2.136 Å for **2**·*S*, whereas those at 110, 175, and 220 K are 1.972/2.013, 1.974/2.056, and 2.100/2.150 Å for **3**·*S*, indicating the presence of a two-step spin crossover in both compounds. Temperature-dependent magnetic susceptibilities ($\chi_M T$) confirm the two-step spin-crossover behavior at 124 and 200 K in **2**·*S*, 151 and 225 K in **3**·*S*, and 51 and 126 K in **4**·*S*, respectively. The frameworks of **2**−**4** are reproducible upon solvent exchange and thereafter undergo solvent-dependent spin-crossover behaviors.

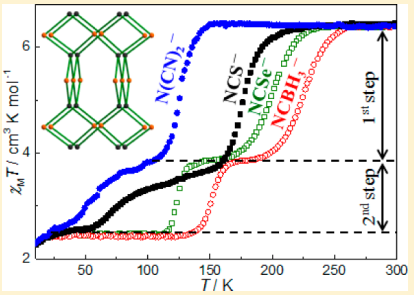

INTRODUCTION

Nowadays, bistable magnetic materials, whose magnetic properties are affected by external physical stimuli, are attracting a broad and sustained attention.[1−7] These materials, including the extensively studied spin-crossover (SCO) compounds,[8−12] represent exceptionally multifunctional materials.[13,14] Up to date, hundreds of SCO compounds have been characterized for their molecular-scale switch between the high-spin (hs) and low-spin (ls) states under external perturbations.[15−18] On the basis of the extensive studies, it has become clear that SCO behavior is fundamentally associated with ligand-field strength as well as intermolecular interactions; the latter may be the essential to observe cooperativity between SCO units.[19−23] For example, guest molecules that could induce weak intermolecular interactions, such as hydrogen bonds and van der Waals interactions, were found to influence the widths of hysteresis loops and thus could be used to evaluate the correlation between SCO behaviors and the host−guest interactions.[24−26] In order to have a deep understanding of solvent effects on SCO properties, the rational design and synthesis of SCO host structures that can reversibly exchange solvent molecules is extremely important.[27,28]

Porous coordination polymers (PCPs) or metal−organic frameworks (MOFs) may meet this demand. They are constructed with organic linkers and inorganic units and are usually two- or three-dimensional structures possessing ordered cavities and/or channels capable of adsorbing solvent (guest) molecules. Therefore, they may be the suitable platform to investigate the effects of host−guest interactions on SCO behaviors[29] when such host structures can undergo spin crossover; that is, the structures contain SCO-active centers. In fact, some efforts have been devoted to introduce SCO-active centers into PCPs or MOFs and to study the effects of solvent molecules on their SCO behaviors.[30,31] Over the course of these studies, it is concluded that notable solvent effects or host−guest interactions might be achieved in structures with small cavity sizes and interpenetrated coordination frameworks, in which the adsorbed solvent molecules can make a significant impact on the intermolecular interactions between solvent and host structure, and thus on SCO behaviors.[23,32,33] This has been exemplified by compound $[Fe(NCS)_2(azpy)_2]\cdot$solvent (azpy = 4,4′-azobispyridine),[34] whose SCO behavior was remarkably affected by the exchangeable solvent molecules. Since then, some SCO-PCP structures showing diverse solvent effects have been reported, and most of them are structurally based on the $Fe^{II}N_6$ chromophore[35−38] and are typically constructed with the $[Fe^{II}(pyridyl)_4(trans\text{-}NCS)_2]$ moiety and bridging exodentate pyridyl-based ligands.[19,20,39,40]

Recently, we have synthesized a 3D SCO-PCP, $[Fe(NCS)_2(tppm)]\cdot S$ (**1**·*S*), using a tetradentate ligand 4,4′,4″,4‴-tetrakis(4-pyridylethen-2-yl)tetraphenylmethane (tppm,

Received: February 27, 2014
Published: April 29, 2014

 © 2014 American Chemical Society dx.doi.org/10.1021/ic500463m | *Inorg. Chem.* 2014, 53, 5246−5252

Scheme 1), and determined its solvent-dependent SCO behavior through introducing various guest molecules in the cavities of the framework.[41] The results indicate that one of the two-step SCO processes (in the higher temperature range) is strongly affected by protic solvents, whereas another (in the lower temperature range) remains intact upon solvent exchange. In this paper, we have synthesized three novel compounds by substituting the NCS^- co-ligand in **1**·*S* with $NCSe^-$ (**2**·*S*), $NCBH_3^-$ (**3**·*S*), and $N(CN)_2^-$ (**4**·*S*), respectively, and report the X-ray diffraction and magnetic studies on these three compounds, aiming at achieving a systematical understanding of solvent as well as co-ligand effects on the SCO behaviors of this system.

Scheme 1. Ligand tppm and Ferrous Salts with Various Co-ligands (X) Used To Synthesize Compounds 2·*S*–4·*S*

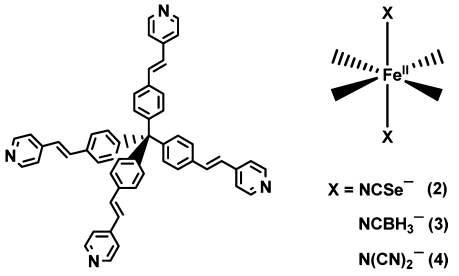

EXPERIMENTAL SECTION

Materials and Physical Measurements. All reagents were obtained from commercial sources and used as received. The ligand 4,4′,4″,4‴-tetrakis(4-pyridylethen-2-yl)tetraphenylmethane (tppm) was synthesized by a literature method.[42] Power X-ray diffraction (PXRD) data were recorded on Panalytical X'pert PRO diffractometer with Cu Kα radiation (λ = 0.15418 nm, 40.0 kV, 30.0 mA) at room temperature. Elemental analyses for C, H, and N were performed on a PerkinElmer 240Q elemental analyzer. IR spectra (KBr pellets) were recorded in the range of 400–4000 cm^{-1} on a Nicolet 5DX spectrophotometer. Magnetic measurements were carried out with a sweeping rate of 1.5 K min^{-1} on a Quantum Design SQUID magnetometer in the 10–300 K temperature range. Magnetic susceptibilities were calibrated with the sample holder, and diamagnetic corrections were estimated from Pascal's constants.

Synthesis. Compounds **2**·*S*, **3**·*S*, and **4**·*S* were synthesized by a diffusion method.[41] Red crystals of **2**·*S* and **3**·*S* suitable for single-crystal X-ray diffraction analysis were obtained in several weeks. The crystalline quality of **4**·*S* does not meet the requirement for single-crystal X-ray diffraction analysis. The total amount of solvent molecules in the molecular formula was determined by elemental and thermogravimetric analyses results. Desolvated samples, **2**–**4**, were obtained by heating the as-synthesized products in vacuum at 50 °C for 2 h.

*[Fe(NCSe)$_2$(tppm)]·5CH$_3$OH·2CH$_2$Cl$_2$ (**2**·*S*).* A CH_2Cl_2 solution (5 mL) of tppm (7.32 mg, 0.01 mmol) was placed in the bottom of a tube, upon which a 10 mL MeOH/CH_2Cl_2 solution (v/v = 1:1.5) was layered; then a MeOH solution (5 mL) of $Fe(NCSe)_2$ (0.01 mmol) was carefully layered. The tube was sealed under nitrogen, and single crystals suitable for X-ray diffraction analysis were obtained in several weeks. Anal. Calcd (%) for $C_{62}H_{64}N_6O_5Cl_4FeSe_2$: C, 56.04; H, 4.855; N, 6.325. Found: C, 56.36; H, 4.669; N, 6.432. Anal. Calcd (%) for the desolvated sample **2** ($C_{55}H_{40}N_6FeSe_2$): C, 66.14; H, 4.037; N, 8.415. Found: C, 65.83; H, 4.258; N, 8.307. IR (cm^{-1}): 3415(s), 3027(w), 2066(s), 1598(s), 1507(s), 1420(m), 1332(w), 1218(w), 1199(w), 1065(w), 1016(m), 968(m), 876(w), 820(s), 654(w), 543(m).

*[Fe(NCBH$_3$)$_2$(tppm)]·5CH$_3$OH·2CH$_2$Cl$_2$ (**3**·*S*).* Anal. Calcd (%) for $C_{62}H_{70}B_2N_6O_5Cl_4Fe$: C, 62.13; H, 5.887; N, 7.012. Found: C, 61.77; H, 5.549; N, 6.642. Anal. Calcd (%) for the desolvated sample **3** ($C_{55}H_{46}B_2N_6Fe$): C, 76.06; H, 5.338; N, 9.677. Found: C, 75.74; H, 5.569; N, 9.601. IR (cm^{-1}): 3427(s), 3026(w), 2070(m), 1598(s), 1507(m), 1420(m), 1383(w), 1218(w), 1199(w), 1065(w), 1016(m), 969(m), 876(w), 821(s), 654(w), 543(s).

*[Fe{N(CN)$_2$}$_2$(tppm)]·5CH$_3$OH·2CH$_2$Cl$_2$ (**4**·*S*).* Anal. Calcd (%) for $C_{64}H_{64}N_{10}Cl_4FeO_5$: C, 61.45; H, 5.157; N, 11.20. Found: C, 60.86; H, 5.469; N, 11.03. Anal. Calcd (%) for the desolvated sample **4** ($C_{57}H_{40}N_{10}Fe$): C, 74.35; H, 4.378; N, 15.21. Found: C, 73.89; H, 4.494; N, 15.55. IR (cm^{-1}): 3406(s), 3028(w), 2267(w), 2157(s), 1598(s), 1507(s), 1420(m), 1332(w), 1217(w), 1200(w), 1120(w), 1065(w), 1016(m), 969(m), 918(w), 877(w), 821(s), 654(w), 542(m).

Solvent Exchange. The as-synthesized products of **2**·*S*–**4**·*S* (~10 mg) were immersed in, respectively, fresh CH_3OH, C_2H_5OH, CH_2Cl_2, $CHCl_3$, CH_3CN, CH_3COCH_3, and C_6H_{12} (20 mL) for 2 h at room temperature. The exchange was conducted for three times, and the crystalline solid was collected by filtration. The amount of solvent molecules in the final samples (named as **2**·*G*–**4**·*G*) was estimated by elemental analysis (Table S1, Supporting Information).

Table 1. Crystal Data and Structural Refinement Parameters for 2·*S* and 3·*S*

	2·*S*			3·*S*		
	100(2) K[a]	155(2) K[a]	220(2) K[a]	110(2) K[a]	175(2) K[a]	220(2) K[a]
formula	$C_{62}H_{64}N_6O_5Cl_4FeSe_2$			$C_{62}H_{70}B_2N_6O_5Cl_4Fe$		
M_r/g mol^{-1}	1328.80			1198.55		
space group	*Pban*	*Pnna*	*Pban*	*Pban*	*Pnna*	*Pban*
a/Å	15.7237(4)	16.9134(7)	17.5637(11)	15.7537(5)	16.9434(6)	17.5817(10)
b/Å	35.9821(7)	40.2990(4)	35.4521(17)	36.0206(8)	40.319(5)	35.4511(13)
c/Å	18.9821(7)	35.5326(13)	20.8450(17)	18.9925(6)	35.6426(11)	20.8530(14)
V/Å^3	10739.7(5)	24219.0(3)	12979.5(15)	10777.4(6)	24349.0(3)	12997.4(12)
Z	4	8	4	4	8	4
D_{calcd}/g cm^{-3}[b]	0.618	0.548	0.511	0.535	0.474	0.444
reflns collected	9223	16 647	10 746	9298	16 745	10 961
unique reflns	3087	4918	3255	3084	4948	3457
F(000)	2024	4048	2024	1816	3632	1816
GOF	0.995	0.980	0.998	0.985	0.996	0.975
R1[c] [$I > 2\sigma(I)$]	0.1086	0.0928	0.1089	0.1036	0.0946	0.1088
wR2[d] (all data)	0.2922	0.2294	0.2877	0.2887	0.2334	0.2867

[a]Temperature. [b]D_{calcd} is obtained based on the solvent-free formula. [c]$R1 = \sum||F_o| - |F_c||/\sum|Fo|$. [d]$wR2 = \{\sum[w(F_o^2 - F_c^2)^2]/\sum[w(F_o^2)^2]\}^{1/2}$.

dx.doi.org/10.1021/ic500463m | Inorg. Chem. 2014, 53, 5246–5252

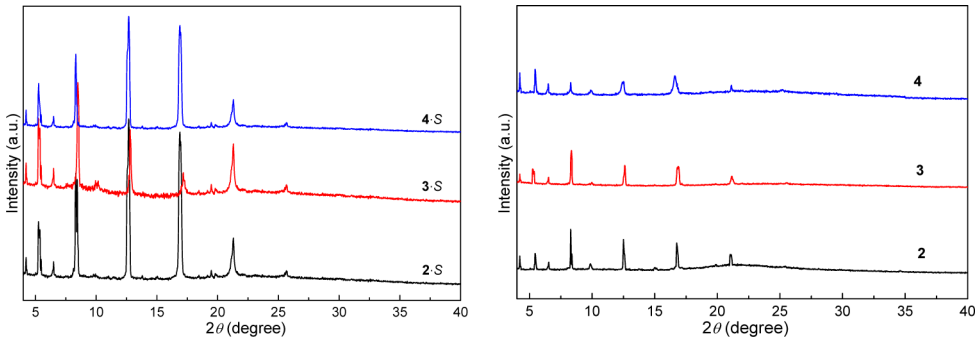

Figure 1. PXRD patterns of **2**·*S*–**4**·*S* (left) and their desolvated samples (right).

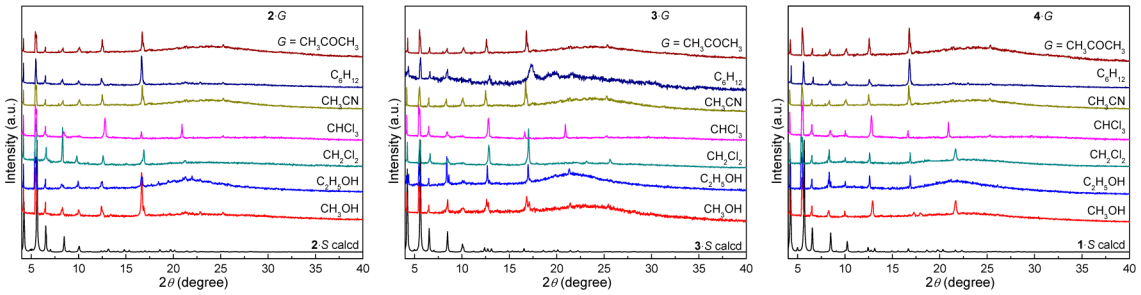

Figure 2. PXRD patterns of **2**·*G*–**4**·*G*. The PRXD patterns simulated from single-crystal structures (**1**·*S*–**3**·*S*) are shown for comparison.

Table 2. Selected Bond Lengths [Å] for 2·*S* and 3·*S*

	2·*S*			3·*S*		
	100(2) K[a]	155(2) K[a]	220(2) K[a]	110(2) K[a]	175(2) K[a]	220(2) K[a]
Fe1–N1	2.040(4)	2.000(4)	2.147(3)	2.043(4)	2.005(4)	2.149(3)
Fe1–N3	1.829(2)	1.981(4)	2.000(2)	1.829(2)	1.986(4)	2.003(1)
Fe1–N5		1.929(1)			1.930(1)	
Fe2–N2	2.097(5)	2.171(4)	2.224(4)	2.100(5)	2.178(4)	2.226(4)
Fe2–N4	1.840(3)	2.154(6)	1.959(2)	1.840(3)	2.158(6)	1.999(2)
Fe2–N6		1.831(1)			1.833(1)	
$<d_{Fe1-N}>$[b]	1.969	1.970	2.098	1.972	1.974	2.100
$<d_{Fe2-N}>$[b]	2.011	2.052	2.136	2.013	2.056	2.150

[a]Temperature. [b]$<d_{Fe-N}>$ is the average Fe–N distance.

X-ray Structure Determination. Single-crystal X-ray diffraction data were recorded on an Agilent SuperNova CCD diffractometer at 100, 155, and 220 K for **2**·*S*, and at 110, 175, and 220 K for **3**·*S*, respectively. The data for **3**·*S* at 220 K were collected using a crystal that has been exchanged with C_2H_5OH, because **3**·*S* itself is of poor quality at the hs state. The structures were solved by direct methods and refined on F^2 by anisotropic full-matrix least-squares methods using SHELXL-97.[43] All non-hydrogen atoms were refined anisotropically, while hydrogen atoms were generated by the riding mode. Electron density contributions from the highly disordered solvent molecules were handled using the "SQUEEZE" procedure from the PLATON software[44] (see details in the Supporting Information). Void volumes are calculated using the "Void" command from the Mercury software.[45,46] Unfortunately, we could not obtain high-quality crystals of **4**·*S* to collect single-crystal X-ray diffraction data; instead, its structure was confirmed to be similar to that of **2**·*S* or **3**·*S* by PXRD studies. A summary of the crystallographic data and refinement parameters is shown in Table 1. CCDC 978303–978308 contain the supplementary crystallographic data, which can be obtained free of charge from the Cambridge Crystallographic Data Center via www.ccdc.cam.ac.uk/data_request/cif.

RESULTS AND DISCUSSION

Synthesis. Crystals of **2**·*S*–**4**·*S* were obtained by a diffusion method in a test tube. The crystal quality is mainly affected by the stoichiometry of reactants and CH_3OH/CH_2Cl_2 ratio; an amount of 0.01–0.05 mmol of tppm and an overall 1:1 ratio of CH_3OH/CH_2Cl_2 (20 mL) would contribute to high-quality crystals of **2**·*S* and **3**·*S* with good yield. However, in this way, the crystal quality of **4**·*S* is still not good enough, and any attempts to improve the crystal quality of **4**·*S* have failed. PXRD studies indicate that the structure of **4**·*S* is similar to those of **2**·*S* and **3**·*S* (Figure 1, left). PXRD studies (Figure 1, right) reveal that the desolvated frameworks remain intact, while thermogravimetric analysis indicates that the structures of **2**–**4** are stable until 300 °C (Figure S1, Supporting Information).

Solvent Exchange. The best way to investigate the solvent effect on SCO behavior is to synthesize compounds that can crystallize out in various solvents, and simultaneously, the crystal encapsulating solvent molecules can be structurally determined by single-crystal X-ray diffraction studies.[37] An alternative way is to carry out solvent exchange to obtain solvent-included compounds. For compounds **2**·*S*–**4**·*S*, we

dx.doi.org/10.1021/ic500463m | Inorg. Chem. 2014, 53, 5246–5252

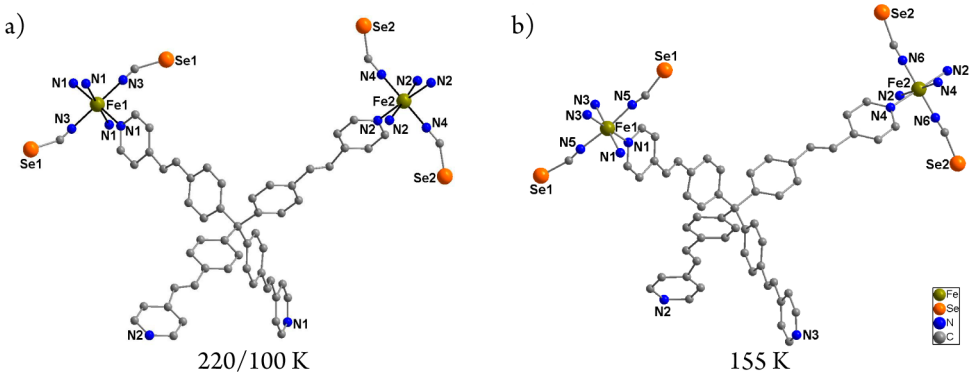

Figure 3. (a, b) Coordination geometries of Fe1 and Fe2 atoms for **2**·*S* at various temperatures.

notice that the framework structures are thermally stable (Figure S1, Supporting Information) and their SCO behaviors are recoverable through a desorption−adsorption process (see below). Therefore, it is feasible to exchange the *S* in crystals of **2**·*S*−**4**·*S* with other solvent molecules, and therefore, solvent effects on SCO behaviors of **2**−**4** can be studied. In fact, the *S* in crystals of **2**·*S*−**4**·*S* is easily exchanged with other solvent molecules by directly immersing crystals of **2**·*S*−**4**·*S* in the respective pure solvents. The resulting products (**2**·*G*−**4**·*G*) have been studied by PXRD, which indicates that the crystallinity and framework structures of **2**·*G*−**4**·*G* remain intact during solvent exchanges (Figure 2).

Crystal Structures. Structure determinations of **2**·*S* and **3**·*S* were carried out under various temperatures in order to correlate the spin states of Fe^{II} centers with structural parameters. Selected bond lengths are summarized in Table 2, and bond angles are shown in Table S2 (Supporting Information).

Compounds **2**·*S* and **3**·*S* crystallize in the orthorhombic space group *Pban* at room temperature. The asymmetric unit of **2** or **3** contains a tetradentate ligand tppm with the central quaternary carbon atom lying on a two-fold axis, two Fe^{II} atoms lying on sites with 222-symmetry, and two co-ligands ($NCSe^-$ in **2**, $NCBH_3^-$ in **3**). As shown in Figure 3a (**2** is shown as the example), each Fe^{II} atom adopts an FeN_6 octahedral coordination geometry with four nitrogen atoms from different tppm ligands located in the basal plane and two nitrogen atoms from $NCSe^-$ groups occupying the apical positions.

When temperatures decrease to 155 K for **2**·*S* and 175 K for **3**·*S*, the space group changes from *Pban* to *Pnna*, which then restores to the initial one (*Pban*) upon further cooling to 100 K; that is, phase transition occurs during spin crossover. Therefore, the two Fe^{II} atoms in the asymmetric unit lie on a two-fold axis at 155 K for **2**·*S* and **3**·*S* (Figure 3b). As shown in Table 2, the average Fe1−N/Fe2−N bond lengths of **2**·*S* are 1.969/2.011, 1.970/2.052, and 2.098/2.136 Å at 100, 155, and 220 K, respectively, while those of **3**·*S* being 1.972/2.013, 1.974/2.056, and 2.100/2.150 Å at 110, 175, and 220 K. These Fe−N distances are within the range of ls and hs-Fe^{II}−N bond lengths in some dinuclear hs−ls and hs−hs SCO Fe^{II} compounds,[47−51] suggesting an incomplete two-step SCO for both compounds.

The three-dimensional structure of **2** or **3** is a two-fold interpenetrated PtS-type (4,4)-connected 3D framework with a Schäfli symbol of (4^2,8^4) (Figure 4). The one-dimensional open channels thus formed along the *a* axis account for about 40% of

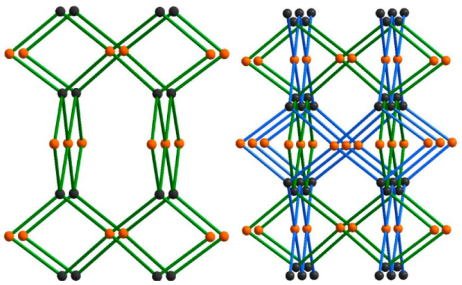

Figure 4. PtS-type topological structure of frameworks **2** and **3** (left) doubly interpenetrates (right) featuring 1D channels along the *a* axis. Orange, Fe^{II}; dark gray, quaternary carbon of tppm.

the unit-cell volume, which are occupied by solvent molecules methanol and methylene chloride.

Magnetic Properties. Magnetic susceptibilities of **2**·*S*−**4**·*S* were recorded in the temperature range of 10−300 K; the $\chi_M T$ (χ_M is molar magnetic susceptibility) versus *T* plots are shown in Figure 5. At room temperature, the $\chi_M T$ values are 6.40−

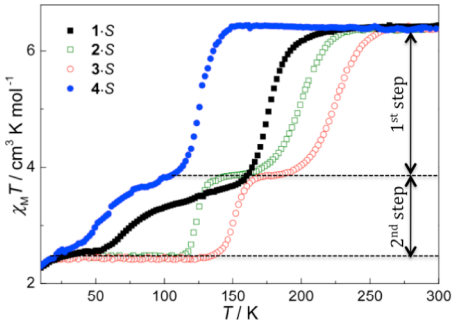

Figure 5. $\chi_M T$ versus *T* plots (per Fe_2 unit) for **2**·*S*−**4**·*S* under an external magnetic field of 5000 Oe. **1**·*S* is shown for comparison.

6.42 cm^3 K mol^{-1} for **2**·*S*−**4**·*S*, corresponding to the value observed for two Fe^{II} ions in the hs−hs state. Upon cooling, the pronounced decreases of $\chi_M T$ values initially begin at 260, 240, and 155 K for **3**·*S*, **2**·*S*, and **4**·*S*, respectively. As mentioned above, the Fe−N bond lengths at different temperatures within the range of ls and hs-Fe^{II}−N bond lengths have shown that **2**·*S*−**4**·*S* undergo an incomplete two-step SCO behavior. The first drop of $\chi_M T$ value spans a range of 2.5−2.8 cm^3 K mol^{-1}, finishing at 186, 161, and 104 K for **3**·*S*, **2**·*S*, and **4**·*S*, respectively. After an inclined plateau, the $\chi_M T$ value of **2**·*S* decreases abruptly from 3.74 cm^3 K mol^{-1} at 132 K to 2.48 cm^3 K mol^{-1} at 113 K, whereas that of **3**·*S* shows a similar, but a

dx.doi.org/10.1021/ic500463m | Inorg. Chem. 2014, 53, 5246−5252

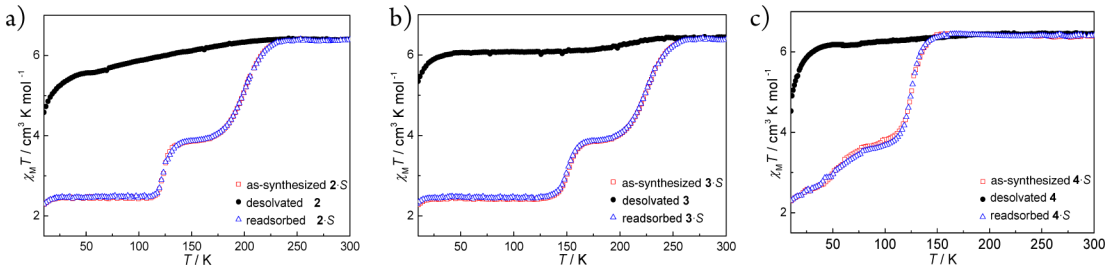

Figure 6. $\chi_M T$ versus T plots (per Fe_2 unit) under an external magnetic field of 5000 Oe for the as-synthesized, desolvated, and readsorbed samples of **2**·*S*–**4**·*S*.

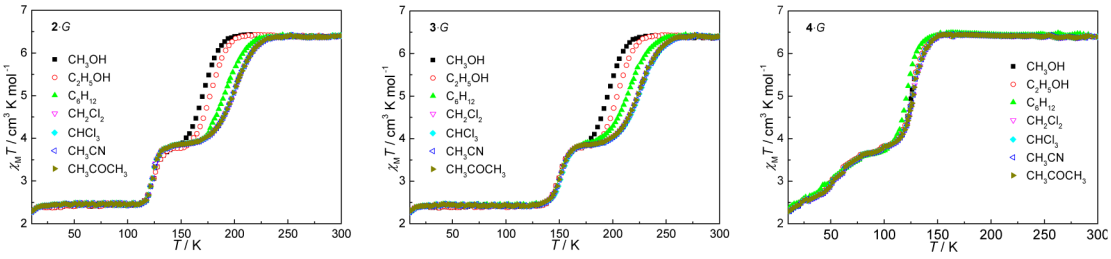

Figure 7. $\chi_M T$ versus T plots (per Fe_2 unit) for **2**·*G*–**4**·*G* as a function of solvents. External magnetic field: 5000 Oe. *G* represents the solvent molecules in frameworks **2**–**4** obtained by solvent exchanges. C_6H_{12} is cyclohexane.

little smooth, behavior, from 3.81 cm^3 K mol^{-1} at 168 K to 2.43 cm^3 K mol^{-1} at 124 K. The second drop of $\chi_M T$ value for **4**·*S* is smoother than those of **2**·*S* and **3**·*S*, showing a total decrease of ~1.0 cm^3 K mol^{-1} from 79 to 31 K. Thus, we can conclude that compounds **2**·*S*–**4**·*S* undergo a two-step incomplete SCO; the critical temperatures $T_{1/2}$(1st)/$T_{1/2}$(2nd), where $T_{1/2}$ is the temperature where the hs and ls species are in equal populations, are 200/124, 225/151, and 126/51 K for **2**·*S*, **3**·*S*, and **4**·*S*, respectively. Taking into account the variable-temperature crystal structures, both Fe^{II} centers in the asymmetric unit may contribute to the first-step SCO and the Fe2 center is mainly responsible for the second-step SCO. Paesani and co-worker[52] have recently interpreted the dependence of $T_{1/2}$ on the nature of the axial ligands NCX^- (X = S, Se, and BH_3) in [Fe(NCX)$_2$(styrylpyridine)$_4$], i.e., $T_{1/2}(NCS^-) < T_{1/2}(NCSe^-) < T_{1/2}(NCBH_3^-)$, in terms of the π-backbonding ability of NCS, NCSe, and $NCBH_3$. This result is consistent with the sequence of ligand-field strength of NCX^-. In the present case (Figure 5), both of the two-step SCO temperatures of compounds **1**·*S*–**3**·*S* follow this principle, whereas, for **4**·*S*, the SCO curve is shifted toward lower temperature, suggesting weaker ligand-field strength for $N(CN)_2^-$.

Before investigation of the tunable solvent-induced SCO behaviors, we have studied the magnetic properties of **2**·*S*–**4**·*S* at different statuses (Figure 6). The fully desolvated samples are no longer sensitive to temperature change and are apparently paramagnetic in the whole temperature range. The sharp decreases of $\chi_M T$ values below 50 K can be assigned to the zero-field effect of paramagnetic hs-Fe^{II} ions. The disappearance of SCO behavior may be due to the loss of host–guest interactions and the deformation of the framework during desolvation.[53] After being immersed in CH_3OH–CH_2Cl_2 (v/v = 1:1) solution, the SCO behaviors are regained and the magnetic curves practically overlap those of the as-synthesized samples, indicating the preservation of frameworks during desorption–adsorption processes and tunable solvent-induced SCO behaviors.

The solvent-exchanged products, **2**·*G*–**4**·*G*, show interesting solvent-dependent SCO behaviors (Figure 7 and Table 3).

Table 3. First-Step SCO Temperature [$T_{1/2}$(1st)] and Volume of Guest Molecule (V)[54,55] for 2·*G*–4·*G*

$T_{1/2}$(1st)/K			
2·*G*	**3**·*G*	**4**·*G*	*V*/Å^3
170	196	126	40.9 (CH_3OH)
178	204	126	60.0 (C_2H_5OH)
190	214	121	101.1 (C_6H_{12})
200	225	126	56.3 (CH_2Cl_2)
199	226	126	69.9 ($CHCl_3$)
201	225	126	52.3 (CH_3CN)
200	224	126	64.4 (CH_3COCH_3)

First, the first-step transitions of **2**·*G* and **3**·*G* with protic solvents methanol and ethanol are apparently shifted toward lower temperature, which can be attributed to the host–guest interactions.[56] Typically, as in methanol, for example, the difference between $T_{1/2}$(1st, **1**·*G*) and $T_{1/2}$(1st, **1**·*S*) ($\Delta T_{1/2}$(**1**) = 42 K)[41] is larger than those between $T_{1/2}$(1st, **2**·*G*) and $T_{1/2}$(1st, **2**·*S*) ($\Delta T_{1/2}$(**2**) = 30 K), and between $T_{1/2}$(1st, **3**·*G*) and $T_{1/2}$(1st, **3**·*S*) ($\Delta T_{1/2}$(**3**) = 29 K). It is speculated that stronger electronegativity of the S atom in NCS^- (**1**·*G*) contributes stronger interactions, such as hydrogen bonds, to protic solvent molecules, than those of Se in $NCSe^-$ (**2**·*G*) and BH_3 in $NCBH_3^-$ (**3**·*G*). Second, the first-step transitions of **2**·*G* and **3**·*G* with aprotic solvents—methylene chloride, chloroform, acetonitrile, and acetone—are hardly affected, though methylene chloride and chloroform may form Cl···S(Se) interactions with NCS^-($NCSe^-$). For the aprotic solvent cyclohexane, both of the first-step transitions of **2**·*G* and **3**·*G* show a moderate shift toward lower temperature ($\Delta T_{1/2} \approx 10$ K for both compounds). As shown in Table 3, the molecular volume of cyclohexane is significantly larger than those of other solvent molecules, so for aprotic solvents, it may be the molecular volume that plays a crucial role in affecting the SCO

dx.doi.org/10.1021/ic500463m | Inorg. Chem. 2014, 53, 5246–5252

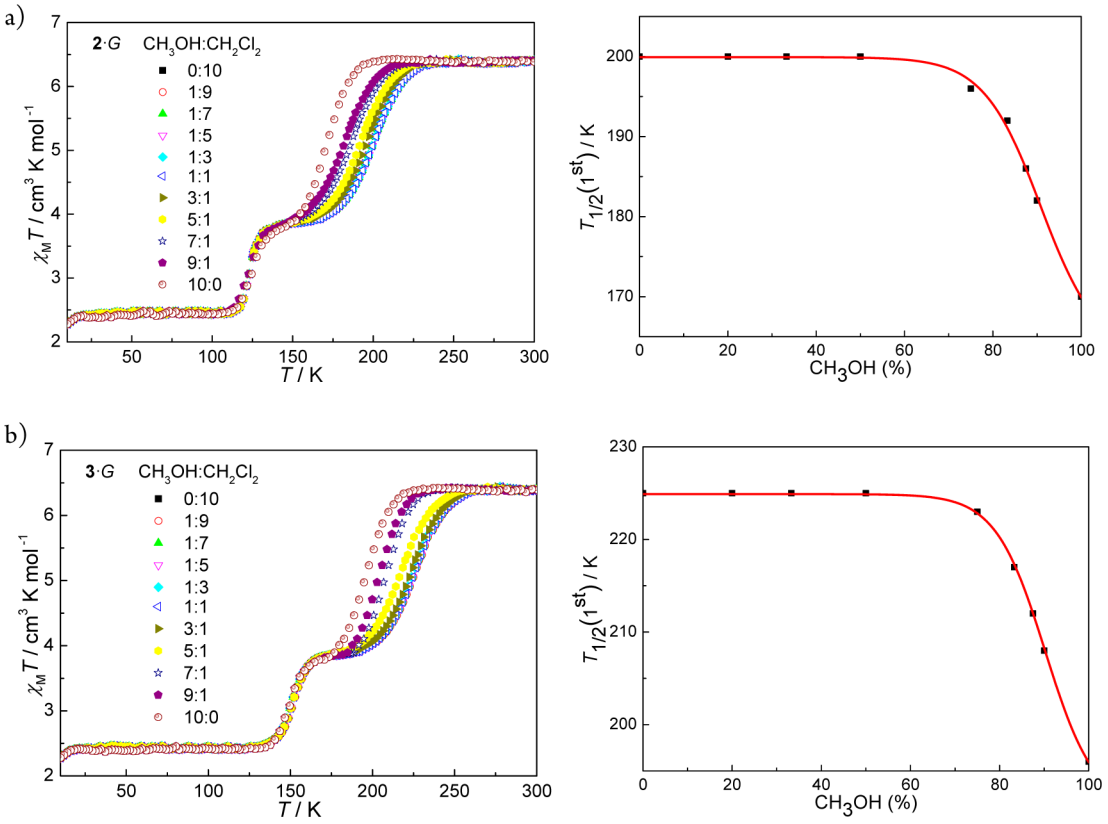

Figure 8. $\chi_M T$ versus T plots (per Fe_2 unit) for **2**·*G* (a, left) and **3**·*G* (b, left) as a function of CH_3OH/CH_2Cl_2 ratio. $T_{1/2}$(1st) versus CH_3OH (v %) in CH_3OH/CH_2Cl_2 solution for **2**·*G* (a, right) and **3**·*G* (b, right). The red solid line represents the best nonlinear regression fit of data.

behavior. That is, large guest molecule prevents the framework from contraction during temperature decreasing.[55] Third, the first-step transition of **4**·*G* is unexpected, almost fixed as a function of solvent ($\Delta T_{1/2}$(**4**) = 0 K) whether it is protic or aprotic, except that only **4**·C_6H_{12} is slightly influenced ($\Delta T_{1/2}$ = 5 K); the reason may be that the first-step transition responsible for relatively visible framework shrinkage can only be affected by guest molecules when it occurs at high temperature, e.g., $T_{1/2}$(1st, **2**·*G*) > 150 K while $T_{1/2}$(1st, **4**·*G*) < 150 K. Fourth, the second-step transitions of samples **2**·*G*−**4**·*G* with various solvents remain unchanged, unveiling that the second-step SCO behaviors are only related to framework stretching, which is resistant to solvent interference after the first-step SCO.

As mentioned above, protic solvent molecules are active and aprotic solvent molecules are passive in affecting the first-step SCO behaviors of **2**·*G* and **3**·*G*. As for mixed protic and aprotic solvents, e.g., a CH_3OH/CH_2Cl_2 mixture, it is expected that the SCO curve will move toward lower temperature with increasing CH_3OH/CH_2Cl_2 ratio. In order to find out the critical CH_3OH/CH_2Cl_2 ratios that essentially affect the first-step SCO behaviors of **2**·*G* and **3**·*G*, quantitative correlations between $T_{1/2}$(1st) and the stoichiometric methanol have been studied. As shown in Figure 8, both samples clearly show similar CH_3OH/CH_2Cl_2 ratio-dependent SCO behaviors. The SCO temperatures are approximately unchanged until the volume percentage of CH_3OH exceeds 50%; then, they remarkably shift to lower temperature along with increasing CH_3OH/CH_2Cl_2 ratios. A fit of the $T_{1/2}$(1st) versus CH_3OH/CH_2Cl_2 ratio plot reveals that a dramatic decrease of $T_{1/2}$(1st) value occurs when the CH_3OH/CH_2Cl_2 ratio is over 70% for either case (Figure 8, right), indicating that only in a high proportion can protic solvent molecules effectively modify SCO behavior of the present system.

CONCLUSIONS

We have reported three two-fold interpenetrated PtS-type porous coordination polymers, **2**·*S*−**4**·*S*, whose SCO behaviors are tunable in the solid state by co-ligands NCX^- [X = Se, BH_3, and $N(CN)_2^-$] and solvent molecules. The SCO temperature is in the order of $T_{1/2}$(**4**·*S*) < $T_{1/2}$(**1**·*S*) < $T_{1/2}$(**2**·*S*) < $T_{1/2}$(**3**·*S*), which is concordant with the sequence of ligand-field strength of co-ligands, i.e., $N(CN)_2^-$ < NCS^- < $NCSe^-$ < $NCBH_3^-$. Among these compounds, **2**·*G* and **3**·*G* show protic solvent-dependent SCO in the first step, whereas **4**·*G* remains intact with any solvents (except cyclohexane). The second-step SCO behaviors of all compounds are unchanged, indicating that they are only induced by thermodynamic factors. The results indicate a possible way toward the optimization of SCO behaviors of sophisticated frameworks with bulky ligands by tuning co-ligands and solvent(guest) molecules.

ASSOCIATED CONTENT

Supporting Information

Crystallographic information in CIF format, elemental analysis results of **2**·*G*−**4**·*G*, and figures. This material is available free of charge via the Internet at http://pubs.acs.org.

AUTHOR INFORMATION

Corresponding Author

*E-mail: taojun@xmu.edu.cn.

dx.doi.org/10.1021/ic500463m | *Inorg. Chem.* 2014, 53, 5246−5252

Notes

The authors declare no competing financial interest.

■ ACKNOWLEDGMENTS

This work was supported by the National Natural Science Foundation of China (Grant 21325103), the "973 project" (2014CB845601), and the Specialized Research Fund for the Doctoral Program of Higher Education (Grant 20110121110012).

■ REFERENCES

(1) Kahn, O.; Kröber, J.; Jay, C. *Adv. Mater.* **1992**, *4*, 718−728.
(2) Sato, O.; Iyoda, T.; Fujishima, A.; Hashimoto, K. *Science* **1996**, *272*, 704−705.
(3) Eddaoudi, M.; Moler, D. B.; Li, H.; Chen, B.; Reineke, T. M.; O'Keeffe, M.; Yaghi, O. M. *Acc. Chem. Res.* **2001**, *34*, 319−330.
(4) James, S. L. *Chem. Soc. Rev.* **2003**, *32*, 276−288.
(5) Janiak, C. *Dalton Trans.* **2003**, 2781−2804.
(6) Kitagawa, S.; Kitaura, R.; Noro, S.-i. *Angew. Chem., Int. Ed.* **2004**, *43*, 2334−2375.
(7) Kepert, C. J. *Chem. Commun.* **2006**, 695−700.
(8) Kahn, O. *Molecular Magnetism*; VCH: New York, 1993.
(9) Gütlich, P.; Goodwin, H. A. In *Spin Crossover in Transition Metal Compounds I*; Gütlich, P., Goodwin, H. A., Eds.; Springer: Berlin, 2004; Vol. *233*, pp 1−47.
(10) Gaspar, A. B.; Ksenofontov, V.; Seredyuk, M.; Gütlich, P. *Coord. Chem. Rev.* **2005**, *249*, 2661−2676.
(11) Real, J. A.; Gaspar, A. B.; Munoz, M. C. *Dalton Trans.* **2005**, 2062−2079.
(12) Sato, O.; Tao, J.; Zhang, Y.-Z. *Angew. Chem., Int. Ed.* **2007**, *46*, 2152−2187.
(13) Miller, J. S. *Inorg. Chem.* **2000**, *39*, 4392−4408.
(14) Miller, J. S., Drillon, M., Eds. *Magnetism: Molecules to Materials II*; Wiley-VCH: Weinheim, Germany, 2002.
(15) Boillot, M.-L.; Zarembowitch, J.; Sour, A. In *Spin Crossover in Transition Metal Compounds II*; Gütlich, P., Goodwin, H. A., Eds.; Springer: Berlin, 2004; Vol. *234*, pp 261−276.
(16) Gütlich, P. In *Spin Crossover in Transition Metal Compounds II*; Gütlich, P., Goodwin, H. A., Eds.; Springer: Berlin, 2004; Vol. *234*, pp 231−260.
(17) Hauser, A. In *Spin Crossover in Transition Metal Compounds II*; Gütlich, P., Goodwin, H. A., Eds.; Springer: Berlin, 2004; Vol. *234*, pp 155−198.
(18) Varret, F.; Boukheddaden, K.; Codjovi, E.; Enachescu, C.; Linarès, J. In *Spin Crossover in Transition Metal Compounds II*; Gütlich, P., Goodwin, H. A., Eds.; Springer: Berlin, 2004; Vol. *234*, pp 199−229.
(19) Garcia, Y.; Niel, V.; Muñoz, M. C.; Real, J. In *Spin Crossover in Transition Metal Compounds I*; Gütlich, P., Goodwin, H. A., Eds.; Springer: Berlin, 2004; Vol. *233*, pp 229−257.
(20) Koningsbruggen, P. In *Spin Crossover in Transition Metal Compounds I*; Gütlich, P., Goodwin, H. A., Eds.; Springer: Berlin, 2004; Vol. *233*, pp 123−149.
(21) Neville, S. M.; Moubaraki, B.; Murray, K. S.; Kepert, C. J. *Angew. Chem., Int. Ed.* **2007**, *46*, 2059−2062.
(22) Kepenekian, M.; Le Guennic, B.; Robert, V. *Phys. Rev.* **2009**, *B79*, 094428.
(23) Kepenekian, M. l.; Guennic, B. L.; Robert, V. *J. Am. Chem. Soc.* **2009**, *131*, 11498−11502.
(24) Niel, V.; Thompson, A. L.; Muñoz, M. C.; Galet, A.; Goeta, A. E.; Real, J. A. *Angew. Chem., Int. Ed.* **2003**, *42*, 3760−3763.
(25) Neville, S. M.; Halder, G. J.; Chapman, K. W.; Duriska, M. B.; Moubaraki, B.; Murray, K. S.; Kepert, C. J. *J. Am. Chem. Soc.* **2009**, *131*, 12106−12108.
(26) Lin, J.-B.; Xue, W.; Wang, B.-Y.; Tao, J.; Zhang, W.-X.; Zhang, J.-P.; Chen, X.-M. *Inorg. Chem.* **2012**, *51*, 9423−9430.
(27) Galet, A.; Munoz, M. C.; Real, J. A. *Chem. Commun.* **2006**, 4321−4323.
(28) Bao, X.; Liu, J.-L.; Leng, J.-D.; Lin, Z.; Tong, M.-L.; Nihei, M.; Oshio, H. *Chem.—Eur. J.* **2010**, *16*, 7973−7978.
(29) Garcia, Y.; Robert, F.; Naik, A. D.; Zhou, G.; Tinant, B.; Robeyns, K.; Michotte, S.; Piraux, L. *J. Am. Chem. Soc.* **2011**, *133*, 15850−15853.
(30) Muñoz, M. C.; Real, J. A. *Coord. Chem. Rev.* **2011**, *255*, 2068−2093.
(31) Olguín, J.; Brooker, S. *Coord. Chem. Rev.* **2011**, *255*, 203−240.
(32) Létard, J.-F.; Guionneau, P.; Goux-Capes, L. In *Spin Crossover in Transition Metal Compounds III*; Gütlich, P., Goodwin, H. A., Eds.; Springer: Berlin, 2004; Vol. *235*, pp 221−249.
(33) Murray, K.; Kepert, C. In *Spin Crossover in Transition Metal Compounds I*; Gütlich, P., Goodwin, H. A., Eds.; Springer: Berlin, 2004; Vol. *233*, pp 195−228.
(34) Halder, G. J.; Kepert, C. J.; Moubaraki, B.; Murray, K. S.; Cashion, J. D. *Science* **2002**, *298*, 1762−1765.
(35) Guionneau, P.; Marchivie, M.; Bravic, G.; Letard, J.-F.; Chasseau, D. *J. Mater. Chem.* **2002**, *12*, 2546−2551.
(36) Li, B.; Wei, R.-J.; Tao, J.; Huang, R.-B.; Zheng, L.-S. *Inorg. Chem.* **2009**, *49*, 745−751.
(37) Wei, R.-J.; Tao, J.; Huang, R.-B.; Zheng, L.-S. *Inorg. Chem.* **2011**, *50*, 8553−8564.
(38) Klingele, J.; Kaase, D.; Klingele, M. H.; Lach, J. *Dalton Trans.* **2012**, *41*, 1397−1406.
(39) Kahn, O.; Codjovi, E. *Philos. Trans. R. Soc., A* **1996**, *354*, 359−379.
(40) Kitchen, J. A.; Brooker, S. *Coord. Chem. Rev.* **2008**, *252*, 2072−2092.
(41) Chen, X.-Y.; Shi, H.-Y.; Huang, R.-B.; Zheng, L.-S.; Tao, J. *Chem. Commun.* **2013**, *49*, 10977−10979.
(42) Cargill Thompson, A. M. W.; Hock, J.; McCleverty, J. A.; Ward, M. D. *Inorg. Chim. Acta* **1997**, *256*, 331−334.
(43) Altomare, A.; Burla, M. C.; Camalli, M.; Cascarano, G. L.; Giacovazzo, C.; Guagliardi, A.; Moliterni, A. G. G.; Polidori, G.; Spagna, R. *J. Appl. Crystallogr.* **1999**, *32*, 115−119.
(44) Spek, A. *Acta Crystallogr.* **2009**, *D65*, 148−155.
(45) Taylor, R.; Macrae, C. F. *Acta Crystallogr.* **2001**, *B57*, 815−827.
(46) Bruno, I. J.; Cole, J. C.; Edgington, P. R.; Kessler, M.; Macrae, C. F.; McCabe, P.; Pearson, J.; Taylor, R. *Acta Crystallogr.* **2002**, *B58*, 389−397.
(47) Ksenofontov, V.; Gaspar, A. B.; Real, J. A.; Gütlich, P. *J. Phys. Chem.* **2001**, *B105*, 12266−12271.
(48) Gaspar, A. B.; Ksenofontov, V.; Real, J. A.; Gütlich, P. *Chem. Phys. Lett.* **2003**, *373*, 385−391.
(49) Real, J. A.; Gaspar, A. B.; Niel, V.; Muñoz, M. C. *Coord. Chem. Rev.* **2003**, *236*, 121−141.
(50) Leita, B. A.; Moubaraki, B.; Murray, K. S.; Smith, J. P.; Cashion, J. D. *Chem. Commun.* **2004**, 156−157.
(51) Fedaoui, D.; Bouhadja, Y.; Kaiba, A.; Guionneau, P.; Létard, J.-F.; Rosa, P. *Eur. J. Inorg. Chem.* **2008**, 1022−1026.
(52) Cirea, J.; Paesani, F. *Inorg. Chem.* **2012**, *51*, 8194−8201.
(53) Neville, S. M.; Halder, G. J.; Chapman, K. W.; Duriska, M. B.; Southon, P. D.; Cashion, J. D.; Létard, J.-F.; Moubaraki, B.; Murray, K. S.; Kepert, C. J. *J. Am. Chem. Soc.* **2008**, *130*, 2869−2876.
(54) Webster, C. E.; Drago, R. S.; Zerner, M. C. *J. Am. Chem. Soc.* **1998**, *120*, 5509−5516.
(55) Southon, P. D.; Liu, L.; Fellows, E. A.; Price, D. J.; Halder, G. J.; Chapman, K. W.; Moubaraki, B.; Murray, K. S.; Létard, J.-F.; Kepert, C. J. *J. Am. Chem. Soc.* **2009**, *131*, 10998−11009.
(56) Brewer, C. T.; Brewer, G.; Butcher, R. J.; Carpenter, E. E.; Schmiedekamp, A. M.; Schmiedekamp, C.; Straka, A.; Viragh, C.; Yuzefpolskiy, Y.; Zavalij, P. *Dalton Trans.* **2011**, *40*, 181−194.